

PACS numbers: 42.60.By; 42.55.Wd; 42.55.Rz; 42.65.Ky; 07.77.Ka
DOI: 10.1070/QE2010v040n12ABEH014435

Laser driver for a photocathode of an electron linear accelerator

A.K. Potemkin, E.I. Gacheva, V.V. Zelenogorskii, E.V. Katin, I.E. Kozhevatov, V.V. Lozhkarev, G.A. Luchinin, D.E. Silin, E.A. Khazanov, G.V. Trubnikov, G.D. Shirkov, M. Kuriki, J. Urakawa

Abstract. **A laser system is designed for operation with a photocathode electron gun for a linear accelerator with the following parameters of radiation at a wavelength of 262 nm (the fourth harmonic of a Nd:YLF laser). The pulse trains (macropulses) with a repetition rate of 5 Hz and a duration of 900 μs consist of 8-ps micropulses with an energy of 1.4 μJ and a repetition rate of 2.708 MHz. This repetition rate is variable within ±32 kHz and is stabilised by an external signal with an accuracy of 10 Hz. Due to the use of a feedback-controlled acousto-optic modulator, the root-mean-square deviation of the micropulse energy in the first and second harmonics is 2.5 % and 3.6 %, respectively. Using the decaying branch of the dependence of the second-to-fourth harmonic conversion efficiency on the second harmonic intensity, we decreased the root-mean-square deviation of the energy of the fourth-harmonic micropulses to 2.3 % at the first-to-fourth harmonic conversion efficiency of 27 %.**

Keywords: *Yb fibre laser, harmonic generation, photoinjector*.

1. Introduction

The project of the International Linear Collider (ILC) includes the creation of an electron – positron collider with a beam energy up to 1 TeV and a brightness of 2×10^{34} cm^{-2} s^{-1} [1]. The ILC will consist of two (electron and positron) linear accelerators based on superconducting RF accelerating units. The RF cavities cooled with liquid helium to 2 K are made of niobium and can operate at electric-field gradients up to 31.5 MV m^{-1}. The accelerators must operate at a macropulse (train) repetition rate of 5 Hz, each macropulse containing 2437 10-ps micropulses spaced by an interval of 369 ns. The repetition rate of these micropulses (2.708 MHz) corresponds to the frequency of the 480th subharmonic of accelerator klystrons operating at 1.3 GHz. One micropulse must carry a charge of 3.2 nC.

At present, the investigations on the Collider are in the stage of development of its components. To refine and demonstrate the technology of production of cryogenic RF electron accelerator modules, the KEK Institute (Japan) has a functioning Super-conducting Test Facility (STF) [2]. As an electron source in its RF electron gun, a photoinjector based on a CsTe cathode is used. The laser system described in this work serves as a light source (laser driver) in the photoinjector. The CsTe photocathode operates in the UV wavelength region and, at a cathode efficiency of 1 % [3], the requirement of a 3.2-nC charge per micropulse corresponds to the laser micropulse energy of 1.5 μJ.

At present, investigations aimed at the creation of photoinjectors are performed in many research centres working on electron linear accelerators. First of all, we should note works of the CERN [3 – 5], the XFEL project [6, 7], and some others [8, 9]. Most laser drivers described in the literature were designed as lasers emitting at the wavelength $\lambda \sim 1$ μm with subsequent conversion to the fourth harmonic [7, 8, 10]. For example, an active laser medium in [7 – 10] was Nd : YLF ($\lambda = 1.047$ μm), and Nd : YAG ($\lambda = 1.064$ μm) was used in [8]. The laser driver described in [9] was based on Ti : sapphire with frequency conversion to the third harmonic.

One of the requirements to laser drivers is a high energy stability both for micropulses inside a macropulse and for macropulses themselves. These problems are solved in different ways. In particular, the laser driver for the CERN operates in a cw regime, whose stability must be maintained by spending a significant part of the pump power. Another drawback of this approach is the impossibility to compensate the time dependence (on the macropulse scale) of the harmonic conversion efficiency caused by thermal effects, because of which the energy stability of micropulses in this case is poor.

In [8], the energy stability of micropulses was achieved using a Pockels-cell placed at the exit of the laser. This scheme also leads to high energy losses. In the laser described in [7], the energy of micropulses was stabilised by controlling the current of lamps pumping the amplifiers. However, the technique used in this case is unreasonably complicated.

All this makes it necessary to develop a compact, reliable, and inexpensive laser driver completely satisfying the requirements imposed on photoinjectors of electron

A.K. Potemkin, E.I. Gacheva, V.V. Zelenogorskii, E.V. Katin, I.E. Kozhevatov, V.V. Lozhkarev, G.A. Luchinin, D.E. Silin, E.A. Khazanov Institute of Applied Physics, Russian Academy of Sciences, ul. Ul'yanova 46, 603950 Nizhnii Novgorod, Russia; e-mail: ptmk@appl.sci-nnov.ru, tzvetochek@list.ru, khazanov@appl.sci-nnov.ru;
G.V. Trubnikov, G.D. Shirkov Joint Institute for Nuclear Research, ul. Zholio Kyuri 6, 141980 Dubna, Moscow region, Russia; e-mail: trubnikov@jinr.ru;
M. Kuriki Hiroshima University, Higashi-Hiroshima, Hiroshima 739-8530, Japan;
J. Urakawa High Energy Accelerator Research Organisation, KEK, 1-1 Oho, Tsukuba, Ibaraki 305-0801, Japan

Received 15 September 2010; revision received 15 October 2010
Kvantovaya Elektronika **40** (12) 1123 – 1130 (2010)
Translated by M.N. Basieva

linear accelerators. The total list of requirements to the parameters of a laser driver for the photoinjector of STF is given below.

Macropulse duration/μs	900
Macropulse fronts/μs	0.3 (at a level of 0.1 – 0.9)
Contrast (the noise-to-micropulse power ratio) for 50 μs	1 : 500
Micropulse duration/ps	8 – 12
Root-mean-square deviation (RMSD) of the micropulse duration (%)	1
Micropulse repetition rate	2.708 MHz ± 1.3 kHz with fluctuations of 50 – 100 Hz
Number of micropulses in a macropulse	2437
Wavelength/nm	260 – 266
Micropulse energy/μJ	1.4
RMSD of micropulse energy (10 successive pulses) (%)	3
RMSD of micropulse energy (in the entire 900-μs pulse) (%)	10

In this work, we describe a driver whose output cascades are based on lamp-pumped rod amplifiers. The master oscillator (MO), preamplifiers (PAs), and the system forming the pulse train envelope in the laser are based on a fibre waveguide.

2. Laser system

Figure 1 shows the optical scheme of a laser driver that can be completely placed on a honeycomb table 220 × 80 cm in size. The driver consists of a fibre section [a fibre MO, an acousto-optic modulator (AOM), and two preamplifiers], a beam-forming scheme (a spatial filter and a soft aperture), a double-pass two-cascade Nd : YLF rod amplifier with a Faraday isolator, and second- and fourth-harmonic generators. Let us consider these units in more detail.

2.1 Master oscillator

As is seen from the above-listed laser driver parameters, rather rigid requirements are imposed both on the energy stability of micropulses in a macropulse and on the micropulse repetition rate. This determined the choice of a fibre laser for the MO. In a fibre laser with an ytterbium-doped waveguide, operating in the self-mode-locked regime without Q-switching, the pulse repetition rate is highly stable and determined only by the optical path length in the cavity. This repetition rate can be easily tuned to the RF accelerator klystron frequency by mechanical stretching of the fibre laser cavity.

As well as in [11], mode locking is performed using a semiconductor saturable mirror (SESAM). To change the pulse repetition rate, we introduced into the MO linear cavity some elements that change its length. The pulse repetition rate is roughly changed by changing the air gap in the cavity, and fine tuning is performed by stretching the active fibre on a piezoelectric cylinder. The rough tuning range is 40.65 – 40.585 MHz, i.e., ±32 kHz, while the fine tuning changes the frequency by ±230 Hz by applying ±200 V to the piezoelectric cylinder. A voltage of 23 V on the piezoelectric cylinder corresponds to one step of the linear translator. Both tuning mechanisms are easily included into the automated cycle of frequency tuning relative to a reference frequency or to an external signal, for example, to the RF signal of the photoinjector cavity.

The pulse repetition rate in a fibre laser fluctuates within a very narrow range (~ 10 Hz). The average pulse repetition rate after a half-hour heating changes insignificantly and only with changing environmental temperature.

The overage output power of the MO was 2 mW, which corresponds to the micropulse energy of 50 pJ. The fluctua-

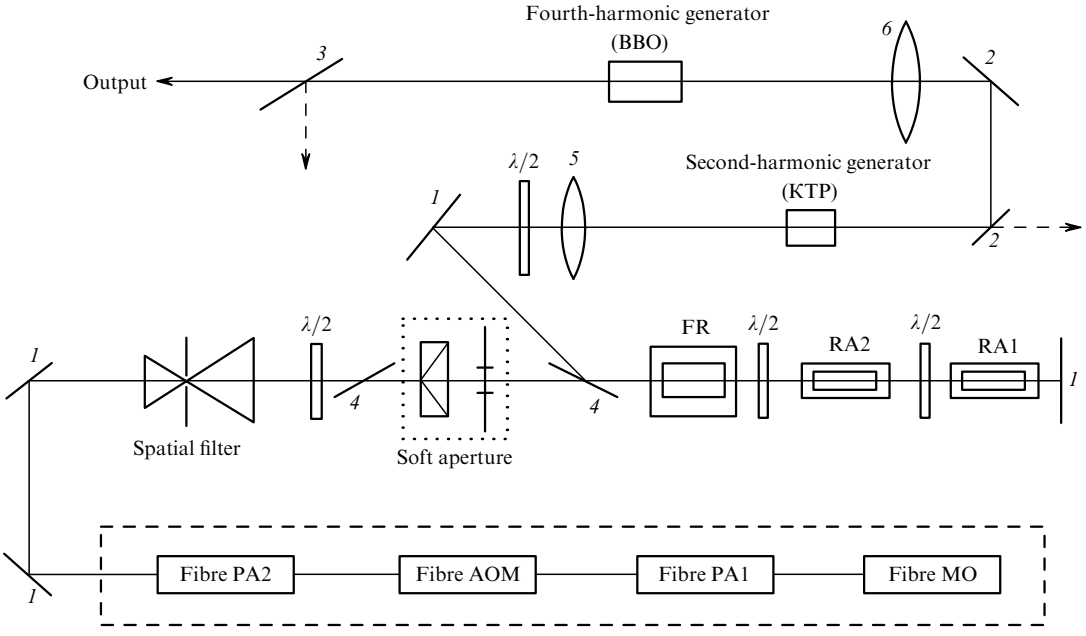

Figure 1. Optical scheme of the laser system: (*1*) mirror ($R = 1$ at $\lambda = 1047$ nm); (*2*) dichroic mirror ($R = 0$ at $\lambda = 1047$ nm, $R = 1$ at $\lambda = 523$ nm); (*3*) dichroic mirror ($R = 0$ at $\lambda = 523$ nm, $R = 1$ at $\lambda = 262$ nm); (*4*) thin-film polarisers; (*5*, *6*) lenses with the focal lengths F_1 and F_2, respectively; (RA1, RA2) rod amplifiers with Nd : YLF AEs (∅5 × 45 mm); (FR) Faraday rotator; (PA1, PA2) preamplifiers; (AOM) acousto-optic modulator.

tions of the average power during four hours did not exceed ±0.5 %.

The duration of micropulses can be estimated from the autocorrelation function (ACF). Figure 2 shows the ACF obtained using an autocorrelator based on SHG in a KDP crystal. This dependence shows that the duration of the Gaussian beam at half maximum is 10 ps [12].

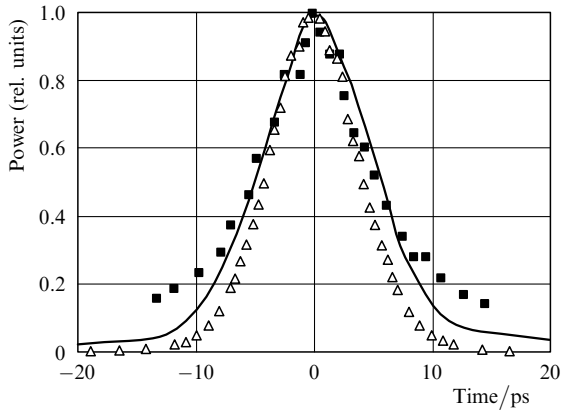

Figure 2. ACFs of the fibre MO pulse (solid curve), of the pulse at the output of the fibre section of the laser (■), and of the second-harmonic pulse (△).

By choosing a Bragg grating, the fibre MO frequency is tuned to the central line of the final Nd : YLF rod amplifier with the π-orientation of the crystal: the optical axis is perpendicular to the rod axis, polarisation is extraordinary, wavelength is $\lambda \sim 1047$ nm (the MO spectrum is given in Fig. 3). The MO bandwidth corresponds to the micropulse duration.

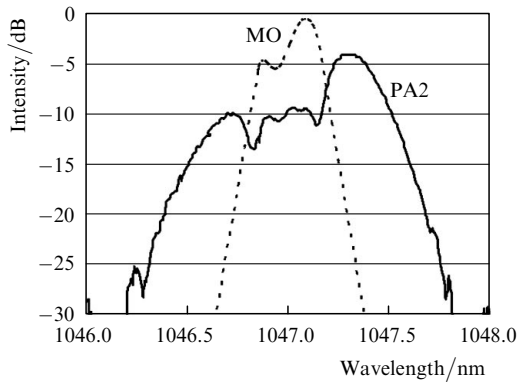

Figure 3. Spectra of radiation emitted from the MO and PA2.

2.2 Fibre preamplifier

The fibre PAs, as well as the fibre MO, are based on a fibre-pumped ytterbium-doped active waveguide. Between the two amplifying cascades (see Fig. 1), we placed an AOM, which provides the following: transmits only each fifteenth pulse and thus decreases the pulse repetition rate to 2.708 MHz, transforms a continuous series of pulses to 900-μs macropulses with a rectangular envelope, and helps to control the macropulse envelope (see below).

At the PA2 exit, i.e., at the exit of the fibre section of the laser, the transverse intensity distribution is almost precisely Gaussian,

$$I(r) = I_0 \exp\left[-\left(\frac{r}{r_0}\right)^2\right]$$

($r_0 = 0.078$ mm). The radiation is linearly polarised with a depolarisation ratio 200 : 1. Then, the depolarised component is coupled out of the scheme by polariser (*4*) (Fig. 1). The beam from PA2 passes a Faraday isolator and a collimator, which forms the beam intensity profile close to Gaussian with a diameter of 5 mm. The output micropulse power of PA2 is as high as 1600 W.

Due to a cubic nonlinearity in the fibre of preamplifiers, the spectrum of the amplified radiation is distorted. At an output micropulse power of 2000 W, the spectrum begins to widen and shift to anti-Stokes wavelengths, because of which we restricted the output power to 1600 W. The spectrum of the PA2 output radiation is shown in Fig. 3. One can see that the linewidth at half maximum increases by a factor of 1.6, which is acceptable for conversion of radiation to the second and fourth harmonics. Nevertheless, the measurements of the ACF (see Fig. 2) showed that the pulse duration of the first harmonic at the exit of PA2 is almost unchanged and, for a Gaussian pulse, is 10 ps at half maximum.

2.3 Beam-forming scheme

The beam-forming unit consists of a spatial filter and an apodising aperture. This unit is needed to adjust the size of the PA2 output beam to the aperture of the rod amplifier and to prevent self-excitation of the entire system.

The spatial filter is a Kepler telescope with an aperture placed in the focal plane. The aperture decreases the parasitic radiation (caused by parasitic reflections, imperfect isolation, luminescence) propagating from the rod amplifier to the PA, which, as a result, prevents the self-excitation of the rod amplifier and the entire laser. A displacement from the confocal positions of the telescope lenses allows one to compensate the quadratic phase component of the PA2 output radiation, which is caused by a thermal lens.

The apodising aperture is described in detail in [13, 14]. It is made of crystalline quartz in the form of a plano-convex lens. A fused silica concave lens attached to the plano-convex lens by optical contact compensates the quadratic component of the radiation wavefront. The Gaussian beam passed through the aperture placed in the immediate vicinity of the rod amplifiers well fills their aperture, which allows one to increase the amplification efficiency.

2.4 Final Nd : YLF rod amplifiers

As was shown above, the maximum peak power of the fibre PA in our case is limited by 1600 W due to the cubic self-focusing, i.e., the PA2 output micropulse energy W is 16 nJ. To increase the radiation energy to a necessary value (see the above-listed requirements to the laser driver parameters), we used two rod amplifiers with Nd : YLF active elements (AEs) (diameter 5 mm, length 90 mm) with the π-orientation.

Each AE is pumped by two pulsed xenon lamps (with the discharge gap 5 mm in diameter and 75 mm in length) loading an oscillating series LC circuit. To decrease the thermal load to AEs, we used two amplifying cascades. The lamps of the amplifiers were discharged with a delay of

500 μs from each other. As was shown by simulation, this scheme is more efficient than the scheme in which both amplifiers start synchronously.

The resistance ρ of the discharge gap (diameter d, length l) of a pulsed lamp nonlinearly depends on the current i flowing through the lamp, $\rho(i) = Ki^{-1/2}$. For a xenon lamp with a working pressure of 300 Torr, $K = 1.27l/d$ [Ω A$^{1/2}$] [15, 16]. For a lamp loading an oscillating LC circuit, the critical discharge, at which the current pulse has a bell-like shape, occurs at the circuit parameter $\alpha_0 = KC^{1/4} \times V_0^{-1/2} L^{-1/4} = 0.8$, where V_0 is the voltage at the capacitor [15]. In this case, the characteristic pulse duration is $\tau = 3\sqrt{LC}$. For the circuit parameters $\alpha_0 \neq 0.8$, the shape of the current pulse will differ from bell-like and can be calculated numerically. Taking into account that the lamp radiation power is $P = Ki^{3/2}$, we can easily calculate the time dependence of the laser gain.

Figure 4 shows the calculated pump radiation power and the gain for the two-cascade double-pass Nd : YLF amplifier. In the calculation, we took into account the lifetime of the laser transition of the active element (490 μs). The constant relating the linear gain with the power supplied to the laser medium was determined experimentally. The experimental data were obtained upon amplification of a rectangular 900-μs pulse emitted by the fibre PA (see section 2.2). As is seen from Fig. 4b, the experimental data well agree with the calculation.

To obtain a rectangular output macropulse, it must be preliminarily distorted to compensate the temporal inhomogeneity of the gain. For this purpose, the AOM-controlling scheme was designed so that it was possible to control the AOM transmission in time. Knowing the experimental shape of the time dependence of the gain and the energy density of the incident radiation, we can calculate such a time dependence of the AOM transmittance at which the shape of the laser output macropulse is rectangular. However, due to an inhomogeneity of the radiation intensity in the plane of the amplifier cross section, these calculations cannot yield a desired accuracy. In this connection, we used an iteration procedure of compensation of the temporal inhomogeneity of the gain. At each iteration (10–20 macropulses), we measured the RMSD of the macropulse energy from the average value. The correction was finished if the RMSD of the macropulse shape from plane did not exceed 2 %.

Figure 4c shows the output macropulses without and with correction. Usually, the reduced shape of a macropulse is achieved after no more than 10 iterations, which takes about one minute of the laser system operation.

The correction is accompanied by losses, which decrease the macropulse energy. However, while the energy incident to the Nd : YLF amplifier decreases by 60 %, the energy at the amplifier output decreases by less than 10 % due to a weaker transition saturation (Fig. 5). Figure 5 also shows that the maximum micropulse energy of 12 μJ is achieved at the electric power of 400 W at each rod, which inevitably leads to the appearance of a thermal lens. This lens was measured using a remote phase-modulation interferometer [17, 18].

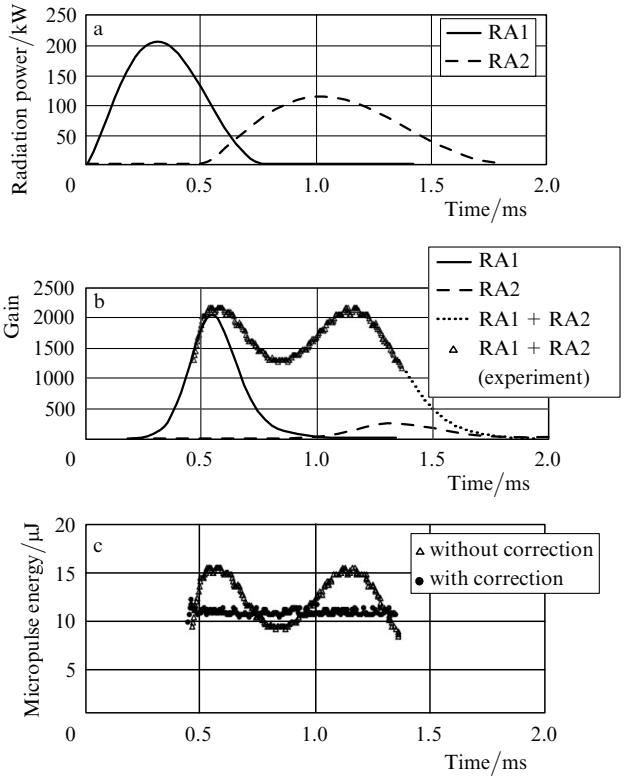

Figure 4. Time dependences of the pump lamp power (a), theoretical (curves) and experimental (points) gains (b), and the micropulse energy at the exit of the two-pass Nd : YLF amplifier without and with correction (c) at $L = 555$ μH, $C = 100$ μF, $U = 1330$ V (RA1) and $L = 1065$ μH, $C = 140$ μF, $U = 1060$ V (RA2).

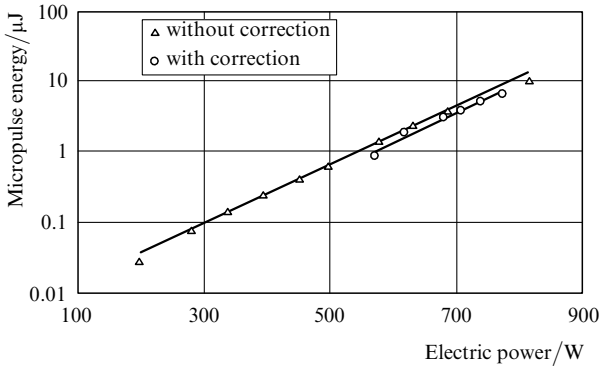

Figure 5. Dependences of the output micropulse energy at the first-harmonic frequency on the electric power of the capacitors of the rod amplifiers without and with correction at the macropulse repetition rate of 5 Hz.

Figure 6 shows the dependence of the thermal lens power on the pump power for two polarisations of light and two directions in space. One can see that the lens in the extraordinary wave used by us is negative and strongly astigmatic. For the maximum power of the two pump lamps of the amplifiers (900 W), the focal length of the lens in two mutually orthogonal directions is −10 and −50 m. As is shown in [19], such a strong astigmatism is explained by the photoelastic effect, whose contribution to the thermal lens is anisotropic. A calculation performed as described in [19] showed that the experimental data coincide with theoretical at the photoelastic coefficients close to those given in this work.

To compensate the astigmatism, we oriented the optical axes of the crystals in the two Nd : YLF amplifiers orthog-

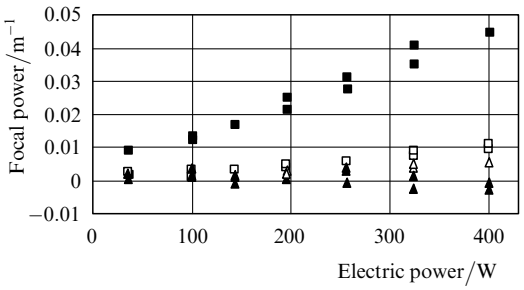

Figure 6. Dependences of the focal power of the thermal lens of one Nd : YLF rod amplifier (diameter 5 mm, length 90 mm) on the electric power of the pump lamps for the ordinary (△, ▲) and extraordinary (□, ■) polarisations in the planes parallel (△, □) and perpendicular (▲, ■) to the optical axis.

onally to each other and placed between them a $\lambda/2$ plate (see Fig. 1), which rotated the polarisation plane by 90°. For identical amplifiers, this method completely eliminates the astigmatism. The remaining quadratic component of the beam wavefront was compensated by the spatial filter telescope or by the lens focusing the beam in the second harmonic generator.

2.5 Second harmonic generator

The fourth harmonic of the laser radiation was achieved in two stages, by frequency doubling and quadrupling. According to the combination of three parameters characterising a crystal (the effective nonlinearity parameter d_{eff}, the angular phase-matching width $\Delta\varphi$, and the spectral phase-matching width $\Delta\lambda$), the best candidate for the second-harmonic generator is the KTP crystal [20].

To determine the crystal length, it is necessary to measure its optical breakdown threshold with respect to the trains of picosecond laser pulses. For this purpose, we placed a 5-mm KTP crystal, which was cut in the direction of the type II phase-matching angle, in the focal plane of a lens with $F_1 = 30$ cm. The input and output faces of the crystal were antireflection coated for the wavelengths of the first ($\lambda = 1047$ nm) and second harmonics, respectively. The intensity distribution in the crystal transverse cross section with the diameter $a = 70$ μm can be assumed to be close to Gaussian, $I(r) = I_0 \exp(-r^2/a^2)$; in this case, the length of the beam waist for the first harmonic will be about 6 cm. The optical breakdown threshold was measured under the phase-matching condition, the second-harmonic generation efficiency being 50 %. A set of our experiments performed in the regime of 900-μs macropulses, each of them consisting of 2347 10-ps micropulses, showed that the breakdown most probably occurs on the output face of the crystal after action of a rather large number of macropulses (from 300 to 3000). The breakdown threshold energy in a macropulse is 130 J cm^{-2}, which corresponds to a micropulse intensity of 5 GW cm^{-2}. The self-focusing causes no noticeable changes in the intensity along the crystal. The estimated maximum value of the B integral is 0.05 and 0.1 for the first and second harmonics, respectively.

Guided by the experimental results considered above, we focused the laser beam into the KTP crystal by a lens with $F_1 = 102.5$ cm to prevent breakdown of the crystal upon frequency doubling. In this case, the energy density in the crystal was an order of magnitude lower than the breakdown threshold density.

As was mentioned above, we eliminated the astigmatism using a half-wave plate placed between the AEs. The remained quadratic component of the wavefront shifts the beam waist position with respect to the focal plane of the lens. Because of this, depending on the macropulse repetition rate, the best results on the SHG are achieved at different distances between the KTP crystal and the lens.

The maximum efficiency in the case shown in Fig. 7 is $\eta_{\max} = 55\,\% - 56\,\%$. It is achieved when the KTP crystal is spaced from the lens by the distance $L = 95$ cm. For the pulse repetition rate of 1 Hz, the maximum efficiency increases to 67 %, but at $L = 85$ cm. The decrease in the efficiency with increasing the repetition rate points to the incomplete compensation of the astigmatism by the half-wave plate and to the presence of high-order thermal aberrations.

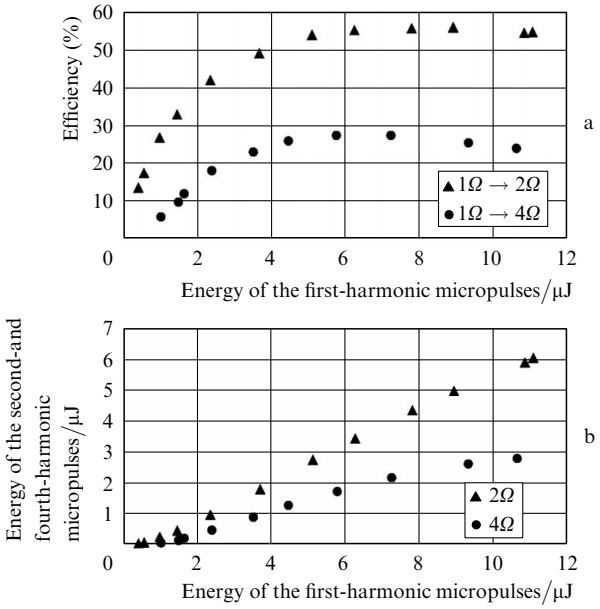

Figure 7. Dependences of the efficiency of conversion of the first harmonic to the second and fourth harmonics (a) and dependences of the second- and fourth-harmonic micropulse energy on the energy of the first-harmonic micropulses (b). The beam radius is 200 and 180 μm in the plane of the KTP and BBO crystal, respectively. SHG occurs in a KTP crystal 75 cm long with a lens with $F_1 = 102.5$ cm; FHG occurs in a BBO crystal 1 cm long with a lens with $F_2 = 30.5$ cm. The macropulse repetition rate is 5 Hz.

We measured the ACF of the second-harmonic radiation by an autocorrelator based on the generation of the second-harmonic of this radiation (the fourth harmonic of the fundamental radiation) in the KTP crystal 5 mm long (see Fig. 2). As is seen, the macropulse duration at the second-harmonic frequency decreases from 10 to 8.5 ps, which is explained by the conversion nonlinearity.

2.6 Fourth-harmonic generator

When choosing the most preferable crystal for the fourth-harmonic generation, one must take into account, in addition to the above-mentioned criteria for efficient SHG, a strong effect of the thermal blooming of the fourth-harmonic radiation. The heat sources upon thermal blooming can be both the linear or two-photon absorption of the fourth-harmonic radiation and the absorption centres

formed inside the crystal [21, 22]. The latter factor may turn out to be especially important. For example, the ADP crystal has a high nonlinear coefficient and a low two-photon absorption coefficient [20]. However, due to the formation of an anomalously high concentration of short-lived absorption centres in this crystal under high-power laser radiation [22], the conversion efficiency may considerably decrease. This phenomenon, which was repeatedly observed by different authors [23, 24], is the main obstacle in using inexpensive high-quality ADP and KTP crystals for cascade generation of the fourth harmonic.

Our experiments with ADP and KTP crystals showed the existence of strong phase distortions appeared when a crystal was precisely oriented in the phase-matching direction. The distortions were observed in the beams of both the second and fourth harmonics and disappeared as the crystal was misaligned from the phase-matching direction. Therefore, we decided in favour of the BBO crystal. The main drawback of this crystal is a large beam deviation angle (85 mrad) [20], which is much higher than in the ADP and KTP crystals.

The BBO crystal 1 cm long was cut along the type I phase matching direction at an angle of 48.8°. The input and output faces were antireflection coated for the wavelengths of the second (523.5 nm) and fourth (262 nm) harmonics, respectively. After reflection from two dichroic 45° mirrors, the second-harmonic beam diverging at an angle close to the diffraction limit was focused by a lens with the focal length $F_2 = 30.5$ cm into the BBO crystal (see Fig. 1). Placing this lens at different distances from the fourth-harmonic generator, it was possible to obtain different energy densities and divergences of the beam in the focal plane of the lens. This specific feature of the focusing system was used to achieve a desired dependence of the fourth-harmonic generation efficiency on the power incident to the crystal (Fig. 7). One can see that the maximum efficiency is 27 % for the first-to-fourth and 49 % for the second-to-fourth harmonic conversion.

A specific feature of the dependence shown in Fig. 7 is that the maximum efficiency is achieved not at the maximum incident energy but at an approximately two-fold lower energy. The region of the right slope was chosen to obtain a stable output power independently of the fluctuations of the first harmonic power. Below we will show the efficiency of this method.

Figure 8 shows the typical images of the fourth-harmonic intensity distributions in the near- (at a distance of ~ 1 m from the BBO crystal) and far-field (in the focal plane of a lens with $F = 50$ cm) zones. Processing of this figure showed that, in the horizontal direction, almost all energy is concentrated in the diffraction angle $1.5\vartheta_{\text{eff}}$. In the vertical direction, there are two maxima propagating at the angle $\vartheta = 3.8\vartheta_{\text{dif}}$.

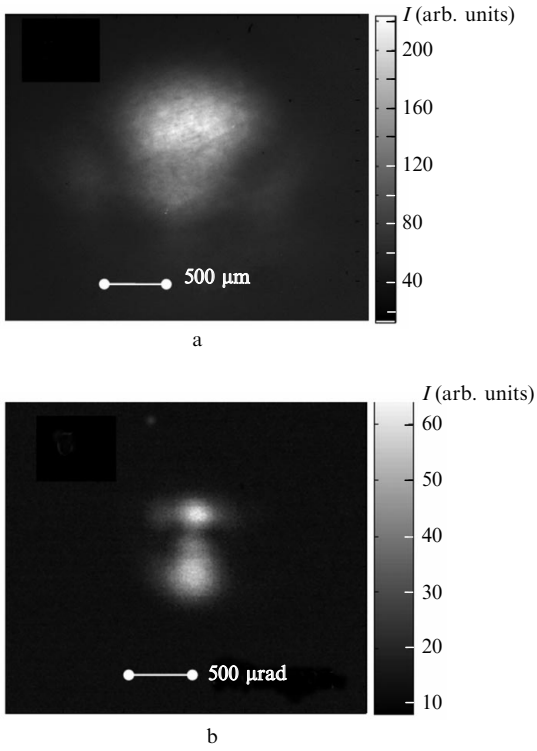

Figure 8. Intensity distribution of the fourth harmonic in the near- (a) and far-field (b) zones at the maximum output power (micropulse energy is 2.6 μJ).

2.7 Macropulse envelope-forming system

As was shown above, due to the temporal inhomogeneity of the gain of the final rod amplifiers, the macropulses emitted by the fibre amplifier are transformed to double-peaked (see Fig. 4). To eliminate this factor, we developed a macropulse envelope-forming system, which controlled the transmission of each of 2437 pulses using an AOM. The controlling signals are generated by a microprocessor analysing the macropulse envelope obtained using a photodiode–oscilloscope–PC chain. Analysing the first-harmonic radiation, we reliably obtain the rectangular shape of only the first-harmonic pulses, but it is not necessary that the envelope of the final output pulse remain rectangular. This is related to the fact that the harmonic conversion efficiency may change during the macropulse due to thermal effects. In the case of correction of the first harmonic pulse envelope, the envelope of the second harmonic pulse also will be almost completely rectangular even at the maximum output power. This points to a weak influence of the thermal blooming in the KTP crystal upon SHG. However, the situation is different in the case of conversion from the second to the fourth harmonic.

Figure 9 presents two pairs of macropulse oscillograms, for correction of the first and fourth harmonics. It is seen that, if we form a good shape of the first harmonic pulse, the pulse of the fourth harmonic shows a nonmonotonic decay. Correcting the fourth harmonic pulse, one can achieve a rectangular shape of this pulse. However, in this case, the energy of the first-harmonic macropulse increases with time, which slightly decreases the efficiency of the entire system, but allows the output pulse to have a rectangular shape. This correction is impossible for systems with the stabilisation of the pulse shape using a quasi-steady-state regime of laser amplification [10].

More pronounced differences in the shapes of the corresponding oscillograms are observed for macropulses with energies 1.5-fold higher than the energies in the case of Fig. 9. This indicates that the thermal blooming threshold energy in the crystal of the fourth-harmonic generator is close to the energy required for a photoinjector (see the above requirements to laser driver parameters). Therefore, to achieve a considerable increase in the energy of macropulses, it is necessary to replace the generator, for example, to use a CLBO crystal [21] instead of BBO.

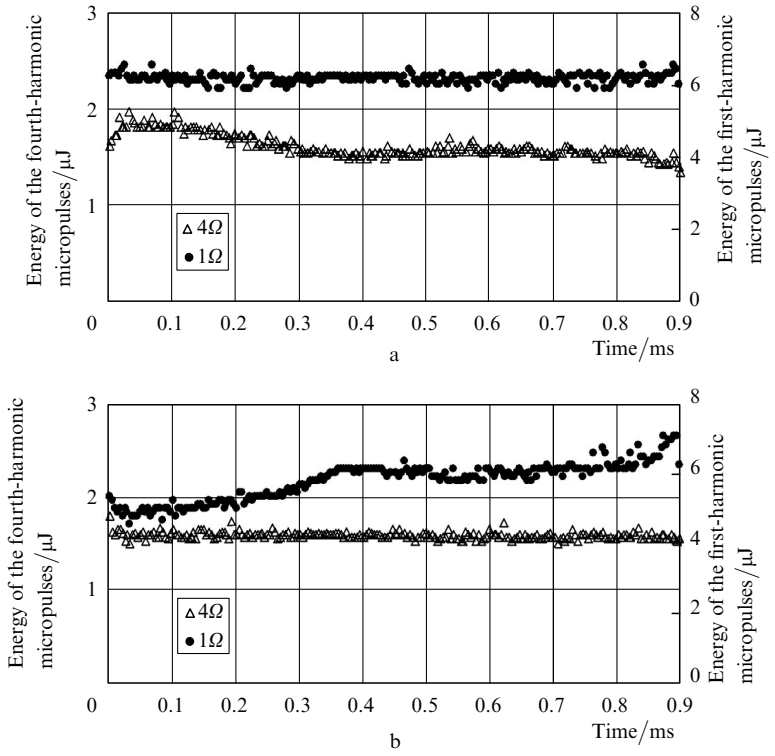

Figure 9. Oscillograms of the first- and fourth-harmonic macropulses with corrections of the shapes of the first (a) and fourth (b) harmonics.

3. Testing of the laser system

The laser system was tested in two ways. First, we determined the average power of radiation in all harmonics during a comparatively short time interval not exceeding 30 min. Second, we measured the gain of the final rod amplifiers for a large time period (about half a year).

The average laser power was measured using a 3A-FS (OPHIR) thermocouple meter. The response time of the meter is 1.8 s, which did not allow us to measure energy in each pulse at the macropulse repetition rate of 5 Hz. Figure 10 shows the time dependences of the micropulse energy in the first, second, and fourth harmonics.

As is seen, the power fluctuations existing in the first harmonic are enhanced in the second harmonic and reduced in the fourth harmonic. Processing of the data given in Fig. 10 showed that RMSD of the power normalised to the average value is 2.5 % for the first, 3.6 % for the second, and 2.3% for the fourth harmonic. For a short time interval of ~ 3 min, the RMSD for the fourth harmonic was 0.5 %. As was noted above, so small fluctuations are achieved due to the generator operation at the decaying branch of the efficiency curve (Fig. 7). Changing the geometry of focusing of the beam into the crystal used in the fourth-harmonic generator, one can increase the conversion efficiency, but the output power fluctuations in this case will be sharply enhanced. The described technique of decreasing the power fluctuations can be also used for the fourth-harmonic generator, but the total decrease in the radiation power in this case will be quite significant.

The laser system endurance is determined mainly by the lamps pumping the final cascades. The lamp endurance, which is characterised by the maximum number of flashes N, is different for operation in the single-pulse and repetitive-pulse regimes. The real endurance will be determined by a

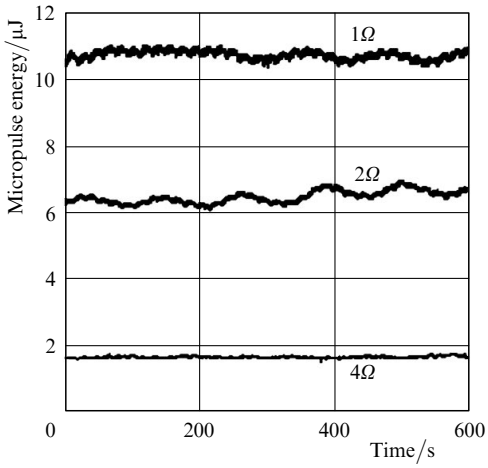

Figure 10. Typical time dependences of the micropulse energy for the first, second, and fourth harmonics at the macropulse repetition rate of 5 Hz.

lower number of flashes. For the energy E of the circuit discharge through a lamp, we will have $N = (E/E_{ex})^{-8.5}$, where $E_{ex} = 22000ld\sqrt{LC}$); here, l and d are the length and diameter of the lamp discharge gap (in cm), while L and C are the inductance and capacity of the discharge circuit [15]. For our case, $N = 10^{10} - 10^{11}$.

For the repetitive-pulse regime, the number N has been determined experimentally and, for lamps constructed similarly to ours, $N = 10^7 - 10^8$ [16], which corresponds to 500 – 5000 h of continuous operation with a pulse repetition rate of 5 Hz. To test the lamps, we measured the gain coefficient of the final amplifiers for half a year. During this time, the lamps operated for about 500 h. We observed no changes in the gain.

4. Conclusions

The proposed architecture and optical scheme of the laser driver for an electron photoinjector ensure a reliable and stable lasing with parameters given in the Introduction. The key ideas that allow one to achieve these output parameters are: the use of a fibre master oscillator with electronically controlled pulse repetition rate; shaping of the preamplifier macropulse using a feedback signal; the use of two Nd : YLF power amplifiers with time-spaced pump pulses and compensation of the thermal lens astigmatism; the reduction of parasitic thermal effects in the fourth-harmonic generator by choosing a BBO crystal and using a computer-controlled feedback that provides the best stability of the macropulse of the forth rather than of the first harmonic.

The principal restriction of a further increase in the energy and pulse repetition rate of micro- and macropulses is the existence of thermal effects accompanying the fourth-harmonic generation. The detailed study of the nature of these effects, as well as of the methods of their suppression and compensation, is the subject of further investigations.

A laser driver for Super-conducting Test Facility (STF) was installed in the KEK Institute (Tsukuba, Japan). At present, it is planned to synchronise it with the RF signal of the STF accelerator, and the driver has everything necessary for this (a fast photodiode, as well as automated rough and fine tuning of the micropulse repetition rate).

Acknowledgements. The authors thank A.V. Andriyanov and S.V. Murav'ev for consultations needed to construct the fibre section of the laser driver.

References

1. Brau J., Okada Y., Walker N. (Eds) *International Linear Collider Reference Design Report ILC Global Design Effort and World Wide Study* (ILC, 2007) V. 1.
2. Tsuchiya K., Higashi Y., Hisamatsu H., Masuzawa M., Matsumoto H., Mitsuda C., Noguchi S., Ohuchi N., Okamura T., Saito K., Terashima A., Toge N., Hayano H. *Proc. EPAC 2006* (Edinburg, Scotland, 2006) p. 505.
3. Braun H.H., Chevallay E., Hutchins S., Legros P., Suberlucq G., Trautner H., Ross I.N., Bente E. *Proc. the Particle Accelerator Conf. 2001* (Chicago, USA, 2001) p. 720.
4. Petrarca M., Braun H.-H., Chevallay E., Doebert S., Elsener K., Fedosseev V., Geschonke G., Losito R., Mas A., Mete O., Rinolfi L., Dabrowski A., Divall M., Champault N., Bienvenu G., Jore M., Mercier B.M., Prevost C., Roux R., Vicario C. *Proc. PAC-09* (Vancouver, Canada, 2009) p. 1.
5. Mete O., Chevallay E., Dabrowski A., Doebert S., Elsener K., Fedosseev V., Lefevre T., Petrarca M., Egger D., Roux R. *Proc. DIPAC-09* (Basel, Switzerland, 2009) p. 104.
6. Altarelli M., Brinkmann R., Chergui M. (Eds) *The European X-ray Free-electron Laser. Techn. Design Report* (Hamburg: DESY XFEL Project Group, 2007).
7. Will I., Liero A., Mertins D., Sandner W. *IEEE J. Quantum Electron.*, **34**, 2020 (1998).
8. Flanchec V., Bleses J., Striby S., Laget J.P. *Appl. Opt.*, **36**, 8541 (1997).
9. Tomizawa H., Dewa H., Hanaki H., Matsui F. *Kvantovaya Elektron.*, **37** (8), 697 (2007) [*Quantum Electron.*, **37** (8), 697 (2007)].
10. Ross I.N., Hutchins S.J. *Central Laser Facility Annual Report 2000/2001* (Chilton, UK: Rutherford Appleton Lab., 2001) p. 184.
11. Turchinovich D., Lui X., Legsgaard J. *Opt. Express*, **16**, 14014 (2008).
12. Ippen E.P., Shank C.V. *Ultrashort Light Pulses Techniques for Measurement* (Berlin, Heidelberg, New York: Springer-Verlag, 1977) p. 2.
13. Kryzhanovskii V.I., Sedov B.M., Serebryakov V.A., Tsvetkov A.D., Yashin V.E. *Kvantovaya Elektron.*, **10** (2), 354 (1983) [*Sov. J. Quantum Electron.*, **13** (2), 194 (1983)].
14. Potemkin A.K., Katin E.V., Kirsanov A.V., Luchinin G.A., Mal'shakov A.N., Mart'yanov M.A., Matveev A.Z., Palashov O.V., Khazanov E.A., Shaikin A.A. *Kvantovaya Elektron.*, **35** (4), 302 (2005) [*Quantum Electron.*, **35** (4), 302 (2005)].
15. Koechner W. *Solid-State Laser Engineering* (Berlin: Springer, 1976).
16. Marshak I.S. (Ed.) *Impul'snye istochniki sveta* (Pulsed Light Sources (Moscow: Energiya, 1978).
17. Zelenogorsky V.V., Solovyov A.A., Kozhevatov I.E., Kamenetsky E.E., Rudenchik E.A., Palashov O.V., Silin D.E., Khazanov E.A. *Appl. Opt.*, **45**, 4092 (2006).
18. Soloviev A.A., Snetkov I.L., Zelenogorsky V.V., Kozhevatov I.E., Palashov O.V., Khazanov E.A. *Opt. Express*, **16**, 21012 (2008).
19. Zelenogorskii V.V., Khazanov E.A. *Kvantovaya Elektron.*, **40** (1), 40 (2010) [*Quantum Electron.*, **40** (1), 40 (2010)].
20. Nikogosyan D.N. *Nonlinear Optical Crystals* (Berlin, Heidelberg: Springer-Verlag, 2005).
21. Ogorodnikov I.N., Pustovarov V.A., Kruzhalov A.V., Isaenko L.I., Kirm M., Tsimmerer G. *Fiz. Tv. Tela*, **42**, 1800 (2000).
22. Ogorodnikov I.N., Yakovlev V.Yu., Shul'gin B.V., Satybaldieva M.K. *Fiz. Tv. Tela*, **44**, 845 (2002).
23. Matos O.M., Torchia G.A., Bilmes G.M., Tocho J.O., Ranea-Sandovas H.F. *Appl. Phys. B*, **80**, 535 (2005).
24. Demos S.G., Staggs M., Radousky H.B. *Phys. Rev. B*, **67**, 224102-1 (2003).